On a nonlinear interpolation procedure and its associated multiresolution scheme

Sergio Amat Plata*

May 11, 2007

Abstract

This paper surveys several topics related to a nonlinear centered piecewise polynomial interpolation technique and the associated multiresolution schemes. This interpolation leads to a nonlinear reconstruction operator with several desirable features: the reconstruction is fourth-order accurate in smooth regions, the data used is always centered with optimal support, the Gibbs phenomenon of linear reconstructions, in the presence of discontinuities, does not appear. Special attention is paid to the stability of the associated multiresolution transform. Finally, some applications are analyzed.

Key Words. Multiresolution, nonlinear subdivision scheme, harmonic mean, signal processing, conservation laws.

AMS(MOS) subject classifications. 41A05, 41A10, 65D05, 65D17

1 Introduction

Recently, various attempts to improve the classical linear multiresolutions of wavelet type have led to nonlinear multiresolutions. In such frameworks, few results for convergence and stability are available [16], [21], [17], [23], [38], [40].

In [9], in the context of image compression, a new multiresolution has been presented. Using a tensorial product, this multiresolution is based

*Departamento de Matemática Aplicada y Estadística. Universidad Politécnica de Cartagena (Spain). Research supported in part by the Spanish grants MTM2004-07114 and 00675/PI/04 and the European network "Breaking complexity" # HPRN-CT-2002-00286. e-mail:sergio.amat@upct.es

on an one dimensional nonlinear multiresolution called PPH (for Piecewise Polynomial Harmonic) multiresolution. It has been analyzed in terms of convergence and stability of its associated subdivision scheme following an approach for data dependent multiresolutions introduced in [21]. Edge resolution, robustness with regard to texture or noise, accuracy and compression capabilities have been numerically investigated. All the results seem to indicate that, opposite to other nonlinear techniques, the PPH multiresolution is stable and can be applied without specific control of error as such introduced in [2].

In [11], we established the stability of the PPH multiresolution that, due to nonlinearity is not a consequence of the stability of the associated subdivision scheme. The key point for that, was to present the PPH multiresolution as some perturbation of a classical linear multiresolution following [28], [40] and [23].

These type of nonlinear reconstructions have several applications as: shock-capturing methods for conservation laws [3], [4], [25], [37], signal processing [1], [5], [14], [12] image and video compression [9], [6], [7], [13], [18] image denoising [8], [39], subdivision schemes [9], [20], [29], [30], [31].

This review paper is organized as follows: In section 2 we present the PPH multiresolution as some perturbation of a linear interpolatory multiresolution. In section 3 we establish a two step contraction property, we deduce a convergence result and prove the stability of the multiresolution. Finally, in section 4 we present and analyze some applications of the PPH reconstruction.

2 The Interpolatory Multiresolution Setting

Let us consider a set of nested grids in $\mathbb{R}$:

$$X^k = \{x_j^k\}_{j\in\mathbb{Z}}, \quad x_j^k = jh_k, \quad h_k = 2^{-k},$$

and the point-value discretization

$$\mathcal{D}_k : \begin{cases} C_B(\mathbb{R}) & \to V^k \\ f & \mapsto f^k = (f_j^k)_{j\in\mathbb{Z}} = (f(x_j^k))_{j\in\mathbb{Z}}, \end{cases} \tag{1}$$

where V^k is the space of real sequences related to the resolution of X^k and $C_B(\mathbb{R})$ the set of bounded continuous functions on $\mathbb{R}$. A reconstruction operator $\mathcal{R}_k$ associated to this discretization is any right inverse of $\mathcal{D}_k$, which means that for all $f^k \in V^k$, $\mathcal{R}_k f^k \in C_B(\mathbb{R})$ and

$$(\mathcal{R}_k f^k)(x_j^k) = f_j^k = f(x_j^k). \tag{2}$$

The sequences $\{\mathcal{D}_k\}$ and $\{\mathcal{R}_k\}$ define a multiresolution transform. The prediction operator, ie, $\mathcal{D}_{k+1}\mathcal{R}_k : V^k \to V^{k+1}$, defines a subdivision scheme. Relation (2) implies that the subdivision scheme is interpolatory (see [15] for details). If $\mathcal{R}_k$ is a nonlinear reconstruction operator, the corresponding subdivision scheme is also nonlinear.

2.1 Linear reconstruction techniques: Data independent Lagrange interpolation

The standard data independent Lagrange interpolatory techniques are used to define *linear* reconstruction operators $(\mathcal{R}_k^{\mathcal{L}} f^k)(x)$ that are piecewise polynomial functions defined in each subinterval $[x_j^k, x_{j+1}^k]$ as the unique interpolation polynomial for the data set $\{f_{j+m}^k, m \in \mathcal{S}\}$ with $\mathcal{S} = \mathcal{S}(r,s) = \{-s, -s+1, \ldots, -s+r\}$.

Lagrange interpolatory techniques lose their accuracy in the presence of isolated singularities. More details can be found in [15].

2.2 Nonlinear reconstruction techniques: PPH interpolation

In this section, we introduce briefly a fourth order non linear and data dependent interpolation scheme based on a piecewise polynomial interpolation operator introduced in [3] and called PPH interpolation. The details can be found in [9].

This nonlinear interpolatory technique leads to a reconstruction operator with several desirable features. First, each polynomial piece is constructed with a fixed centered stencil of 4 points $\{x_{j-1}^k, x_j^k, x_{j+1}^k, x_{j+2}^k\}$. Second, the reconstruction is as accurate as its linear equivalent on smooth regions. Third, the accuracy is reduced close to singularities, but it is not completely lost as in its linear counterpart.

Considering the divided differences associated to the interpolatory stencil,

$$e_{j-\frac{1}{2}}^k = f[x_{j-1}^k, x_j^k], \qquad e_{j+\frac{1}{2}}^k = f[x_j^k, x_{j+1}^k], \qquad e_{j+\frac{3}{2}}^k = f[x_{j+1}^k, x_{j+2}^k],$$

$$D_j^k = f[x_{j-1}^k, x_j^k, x_{j+1}^k], \qquad D_{j+1}^k = f[x_j^k, x_{j+1}^k, x_{j+2}^k],$$

the PPH interpolation from the centered data $f_{j-1}^k, f_j^k, f_{j+1}^k, f_{j+2}^k$ has the following form

$$\tilde{P}_j(x_{j+\frac{1}{2}}^k) = \frac{f_j^k + f_{j+1}^k}{2} - \frac{1}{4}\tilde{D}^k h^2. \tag{3}$$

where

$$\tilde{D}^k = \begin{cases} \frac{2D_j^k D_{j+1}^k}{D_j^k + D_{j+1}^k} & \text{if } D_j^k D_{j+1}^k > 0, \\ 0 & \text{otherwise.} \end{cases} \tag{4}$$

It is interesting to compare this expression with the equivalent one obtained from the centered Lagrange interpolatory polynomial $P_j(x)$

$$P_j(x^k_{j+\frac{1}{2}}) = \frac{f_j^k + f_{j+1}^k}{2} - \frac{1}{4}\frac{D_j^k + D_{j+1}^k}{2}h^2. \tag{5}$$

Due to the fact that

$$|2\frac{D_j^k D_{j+1}^k}{D_j^k + D_{j+1}^k}| \leq 2\min(|D_j^k|, |D_{j+1}^k|) = O(1), \tag{6}$$

we obtain $\tilde{D}^k = O(1)$, instead of $O(\frac{1}{h})$, as in the linear case when a discontinuity exists in $[x^k_{j-1}, x^k_j]$ or in $[x^k_{j+1}, x^k_{j+2}]$.

We notice that the net effect is the replacement of the arithmetic mean of D_j^k and D_{j+1}^k by the 'modified' harmonic mean $\tilde{D}^k$ in (4). The arithmetic mean and the harmonic mean of two values are very close for values of the same magnitude, but the harmonic mean is always bounded in absolute value by twice the absolute value of the smallest of the two numbers. This property is the key to the behavior of the PPH reconstruction close to isolated singularities.

Other two reformulations of the proposed modification, derived from elementary algebra, that are useful for the theoretical analysis, can be found in [9].

We establish next some properties of the PPH reconstruction operator:

1) By construction, the data used for the interpolation remain centered.

2) The reformulations show that our scheme involves a nonlinear modification of the values f^k_{j-1} or f^k_{j+2}, ie, the values at the boundary of the 4-point stencil.

3) If f is a polynomial of degree less or equal to 2,

$$D_j^k = D_{j+1}^k = \frac{D_j^k + D_{j+1}^k}{2} = \tilde{D}^k,$$

therefore the proposed scheme reproduces polynomials of degree 2.

4) If $f \in C^4$ and $D_j^k D_{j+1}^k > 0$, using a Taylor expansion we get

$$\begin{aligned} 2\frac{D_j^k D_{j+1}^k}{D_j^k + D_{j+1}^k} &= \frac{f''(x^k_{j+\frac{1}{2}})}{2} + O(h^2), \\ \frac{D_j^k + D_{j+1}^k}{2} &= \frac{f''(x^k_{j+\frac{1}{2}})}{2} + O(h^2). \end{aligned}$$

Therefore, in smooth regions, the difference between the arithmetic mean and the harmonic mean is $O(h^2)$, hence the proposed reconstruction remains fourth order accurate in smooth regions.

5) When $D_j^k D_{j+1}^k \leq 0$, $\tilde{P}(x^k_{j+1/2}) = \frac{f^k_{j+1}+f^k_j}{2}$. In this case, the accuracy of the reconstruction is limited to second order even in smooth regions.

6) If there is a discontinuity in $[x^k_{j+1}, x^k_{j+2}]$ and $D_j^k D_{j+1}^k > 0$, due to (6) the Gibbs phenomenon of linear reconstruction does not appear. In addition, the order of accuracy of the reconstruction remains $O(h^2)$ in this case.

For more details see [9], [44].

3 Stability of the PPH multiresolution

Introducing the differences $D^k f_j = f^k_{j+1} - 2f^k_j + f^k_{j-1}$, according to section 2, the PPH reconstruction, $\tilde{P}_j$ when $|D^k f_j| \leq |D^k f_{j+1}|$, is the polynomial of degree 3 defined by

$$\begin{cases} \tilde{P}_j(x^k_l) &= f^k_l, \quad \text{for } j-1 \leq l \leq j+1, \\ \tilde{P}_j(x^k_{j+2}) &= \tilde{f}^k_{j+2}, \end{cases} \tag{7}$$

with

$$\tilde{f}^k_{j+2} = f^k_{j+1} + f^k_j - f^k_{j-1} + 2H(D^k f_j, D^k f_{j+1}),$$

where H is defined by:

$$(x,y) \in I\!R^2 \mapsto H(x,y) := \frac{xy}{x+y}(\text{sgn}(xy)+1), \tag{8}$$

where $\text{sgn}(x) = 1$ if $x \geq 0$ and $\text{sgn}(x) = -1$ if $x < 0$.

Before establishing the stability, we need the following technical lemmas that deal with the function H defined above. We refer [11] for the details.

Lemma 1 *For any couples $(x,y),(x',y') \in \mathbb{R}^2$, the function H satisfies the following properties:*

1) $H(x,y) = H(y,x)$

2) $H(x,y) = 0$ if $xy \leq 0$

3) $H(-x,-y) = -H(x,y)$

4) $|H(x,y)| \leq \max(|x|,|y|)$

5) $|H(x,y)| \leq 2\min(|x|,|y|)$

6) $|H(x,y) - H(x',y')| \leq 2\max\{|x-x'|,|y-y'|\}$.

Lemma 2 *The function Z defined on $\mathbb{R}^3$ by $Z(x,y,z) = \frac{x}{2} - \frac{1}{8}(H(x,y) + H(x,z))$ satisfies the following properties:*

1) $|Z(x,y,z)| \leq \frac{|x|}{2}$

2) $sign(Z(x,y,z)) = sign(x)$.

3) $|Z(x,y,z) - Z(x^{'},y^{'},z^{'})| \leq \frac{1}{2}|x-x^{'}| + \frac{1}{2}\max\{|y-y^{'}|,|z-z^{'}|\}$

We then focus on the subdivision scheme S_{PPH} associated to the PPH prediction that writes

$$f^{k-1} \mapsto S_{PPH}(f^{k-1}) = \mathcal{D}_k \mathcal{R}_{k-1} f^{k-1},$$

with

$$\begin{cases} (\mathcal{D}_k \mathcal{R}_{k-1} f^{k-1})_{2j+1} = \tilde{P}_j(x^k_{j+\frac{1}{2}}), \\ (\mathcal{D}_k \mathcal{R}_{k-1} f^{k-1})_{2j} = f^{k-1}_j. \end{cases} \tag{9}$$

We have the following two step contraction property:

Proposition 1 *If, removing k for simplicity, $\hat{f} = S_{PPH}(f)$, $\hat{g} = S_{PPH}(g)$, $\bar{f} = S_{PPH}(\hat{f})$ and $\bar{g} = S_{PPH}(\hat{g})$ then*

$$\begin{array}{lll} 1) & ||D\hat{f}||_{l_\infty(\mathbb{Z})} \leq \frac{1}{2}||Df||_{l_\infty(\mathbb{Z})}, & \\ 2) & |D(\hat{f}_j - \hat{g}_j)| \leq \frac{1}{2}||D(f-g)||_{l_\infty(\mathbb{Z})}, & \text{for } j = 2n+1, \\ & |D(\hat{f}_j - \hat{g}_j)| \leq ||D(f-g)||_{l_\infty(\mathbb{Z})}, & \text{for } j = 2n, \\ \text{and} & & \\ 3) & ||D(\bar{f} - \bar{g})||_{l_\infty(\mathbb{Z})} \leq \frac{3}{4}||D(f-g)||_{l_\infty(\mathbb{Z})}. & \end{array} \tag{10}$$

REMARK 3.1 *The following example,* $(D^k f_n, D^k f_{n+1}, D^k f_{n-1}) = (M+1, 0, 0)$ *and* $(D^k g_n, D^k g_{n+1}, D^k g_{n-1}) = (M, 1, 1)$ *with* $M \to +\infty$ *shows that a single step contraction property in the sense of property 2)* ($j = 2n+1$) *of proposition 1 is not available for* $j = 2n$.

We are now able to derive directly the convergence of the subdivision scheme[1] S_{PPH}, applying theorem 3.3 of [23]. In our context, this theorem applies as follows: If S_L is a converging linear subdivision scheme with Hölder smoothness s_L, reproducing polynomials up to degree P, if S_N is a perturbation of S_L in the sense that, calling $f^k := S_N(f^0)$ for all $f^0 \in l_\infty$,

$$||S_N(f^k) - S_L(f^k)||_{l_\infty(\mathbb{Z})} = O(2^{-\nu k}),$$

then S_N is convergent with an Hölder smoothness $s_N \geq \min(P, s_L, \nu) - \delta$ for all $\delta > 0$.

Indeed, if we choose $S_{\mathcal{L}}$, the linear interpolatory subdivision scheme for S_L (see (3)), we have $s_L = 1$ and from property 3) of lemma 1 and Proposition 1, $\nu = 1$. With $P = 1$ we obtain the convergence of S_{PPH} with Hölder regularity $1 - \delta$.

REMARK 3.2 *It is shown in [36] that the limit curves obtained under* S_{PPH} *are at most Lipschitz continuous* ($s = 1$) *as it can be observed considering the Dirac delta sequence* $f^0 = (..., 0, 0, 1, 0, 0, ...)$. *Indeed, its limit curve is a piecewise linear hat function.*

REMARK 3.3 *Using other tracks, a general approach in [21] and [9] or convexity preservation in [36] and [32], the convergence for the subdivision scheme* S_{PPH} *has been established. However, this property is not sufficient to ensure the stability of the associated multiresolution. The ENO-interpolatory subdivision scheme [21], constructed, as the PPH, in the Harten's framework and involving data dependent linear interpolation, is an example of converging but unstable non linear subdivision scheme.*

We now consider the PPH multiresolution.

We first give the following result involving the details $d(f), d(g)$ and $d(\dot{f}), d(\dot{g})$:

[1] A subdivision scheme S is called convergent with Hölder smoothness s if, for all sequence $f^0 \in l_\infty(\mathbb{Z})$, the sequence of piecewise linear functions ϕ^k interpolating the points f_j^k at x_j^k converges to a function ϕ of Hölder regularity s.

Proposition 2 *If, removing k for simplicity,* $\dot{f} = S_{PPH}(f) + d(f)$, $\dot{g} = S_{PPH}(g) + d(g)$, $\ddot{f} = S_{PPH}(\dot{f}) + d(\dot{f})$ *and* $\ddot{g} = S_{PPH}(\dot{g}) + d(\dot{g})$ *then*

$$
\begin{array}{ll}
1) & ||D\dot{f}||_{l_\infty(\mathbb{Z})} \leq \frac{1}{2}||Df||_{l_\infty(\mathbb{Z})} + ||Dd(f)||_{l_\infty(\mathbb{Z})}, \\
2) & |D(\dot{f}_j - \dot{g}_j)| \leq \frac{1}{2}||D(f-g)||_{l_\infty(\mathbb{Z})} + ||Dd(f) - Dd(g)||_{l_\infty(\mathbb{Z})}, \quad \textit{for } j = 2n+1, \\
 & |D(\dot{f}_j - \dot{g}_j)| \leq ||D(f-g)||_{l_\infty(\mathbb{Z})} + ||Dd(f) - Dd(g)||_{l_\infty(\mathbb{Z})}, \quad \textit{for } j = 2n, \\
\textit{and} & \\
3) & ||D(\ddot{f} - \ddot{g})||_{l_\infty(\mathbb{Z})} \leq \frac{3}{4}||D(f-g)||_{l_\infty(\mathbb{Z})} \\
 & \qquad + ||Dd(f) - Dd(g)||_{l_\infty(\mathbb{Z})} + ||Dd(\dot{f}) - Dd(\dot{g})||_{l_\infty(\mathbb{Z})}.
\end{array}
\tag{11}
$$

We are then able to establish the following theorem related to the stability of the PPH multiresolution $\{f^0, d^0, \ldots, d^{L-1}\} \mapsto f^L$:

Theorem 1 *For any pair of elements* $f^L, \widetilde{f}^L \in l_\infty(\mathbb{Z})$ *and their PPH decompositions* $\{f^0, d^0, \ldots, d^{L-1}\}$ *and* $\{\widetilde{f}^0, \widetilde{d}^0, \ldots, \widetilde{d}^{L-1}\}$, *we have:*

$$
||f^L - \widetilde{f}^L||_{l_\infty(\mathbb{Z})} \leq 9 \left(||f^0 - \widetilde{f}^0||_{l_\infty(\mathbb{Z})} + \sum_{k=0}^{L-1} ||d^k - \widetilde{d}^k||_{l_\infty(\mathbb{Z})} \right). \tag{12}
$$

Finally, we have a last theorem related to the stability of the PPH decomposition $f^L \mapsto \{f^0, d^0, \ldots, d^{L-1}\}$:

Theorem 2 *Given* $\{f^0, d^0, \ldots, d^{L-1}\}$ *and* $\{\widetilde{f}^0, \widetilde{d}^0, \ldots, \widetilde{d}^{L-1}\}$ *two PPH decompositions, corresponding to* $f^L, \widetilde{f}^L \in l_\infty(\mathbb{Z})$, *then*

$$
\begin{array}{rcl}
||f^0 - \widetilde{f}^0||_{l_\infty(\mathbb{Z})} & \leq & ||f^L - \widetilde{f}^L||_{l_\infty(\mathbb{Z})}, \\
||d^k - \widetilde{d}^k||_{l_\infty(\mathbb{Z})} & \leq & 3\ ||f^L - \widetilde{f}^L||_{l_\infty(\mathbb{Z})},\ \forall 0 \leq k \leq L-1.
\end{array}
$$

The proofs of all these results can be found in [11].

4 Applications

In this section we review several applications of the PPH reconstruction.

4.1 Shock capturing methods for hyperbolic conservation laws

We consider numerical approximations to weak solutions of nonlinear hyperbolic conservation laws:

$$u_t + f(u)_x = 0, \tag{13}$$

$$u(x,0) = u_0(x). \tag{14}$$

where the initial data $u_0(x)$ are supposed to be piecewise smooth functions either periodic or of compact support.

Let be $u_j^n = u_h(x_j, t_n)$ denote a numerical approximation to the exact solution $u(x_j, t_n)$ of (13)-(14) defined on a computational grid $x_j = jh$, $t_n = n\Delta t$ in conservation form:

$$u_j^{n+1} = u_j^n - \lambda(\hat{f}^n_{j+\frac{1}{2}} - \hat{f}^n_{j-\frac{1}{2}}), \tag{15}$$

where $\lambda = \frac{\Delta t}{h}$ and the numerical flux is a function of 2k variables

$$\hat{f}^n_{j+\frac{1}{2}} = \hat{f}(u^n_{j-k+1}, \ldots, u^n_{j+k}), \tag{16}$$

which is consistent with (13), i.e.

$$\hat{f}(u, \ldots, u) = f(u). \tag{17}$$

The importance of the following lemma is because it implies that approximating the numerical flux $\hat{f}_{j+\frac{1}{2}}$ to a high order accuracy it is enough to reconstruct $g(x_{j+\frac{1}{2}})$ (see equation (18)) up to the same order.

Lemma 3 (Shu and Osher) *If a function $g(x)$ satisfies*

$$f(u(x)) = \frac{1}{h}\int_{x-\frac{h}{2}}^{x+\frac{h}{2}} g(\xi)d\xi \tag{18}$$

then

$$f(u(x))_x = \frac{g(x+\frac{h}{2}) - g(x-\frac{h}{2})}{h}.$$

We define a computational grid $x_j = jh$, j integer, $h > 0$, where the cells are

$$C_j = \{x : x_{j-\frac{1}{2}} \leq x \leq x_{j+\frac{1}{2}}\}, \tag{19}$$

and $x_{j+\frac{1}{2}} = x_j + \frac{1}{2}h$.

Our grid data are:

$$v_j = \frac{1}{h}\int_{x_{j-\frac{1}{2}}}^{x_{j+\frac{1}{2}}} g(\xi)d\xi, \tag{20}$$

$$d_{j+\frac{1}{2}} = \frac{v_{j+1} - v_j}{h}, \tag{21}$$

$(d_{j+\frac{1}{2}} = g^{'}(x_{j+\frac{1}{2}}) + O(h^2))$.

We required the following conditions for every j:

$$v_j = \frac{1}{h}\int_{x_{j-\frac{1}{2}}}^{x_{j+\frac{1}{2}}} r_j(\xi)d\xi, \tag{22}$$

$$d_{i+\frac{1}{2}} = r_j^{'}(x_{i+\frac{1}{2}}),\ i = j-1, j. \tag{23}$$

Taylor series expansions show that conditions (22) and (23) imply third order accuracy of the reconstruction $r_j(x)$.

The reconstruction procedure is repeated at every time step, thus the change in total variation of the reconstruction must be controlled.

The algorithm defines the modified reconstruction $\tilde{r}_j(x)$ such that its derivative interpolates d_j at x_j and the lateral grid derivative with smallest absolute value. Where, if C_j is a nontransition ($d_{j-\frac{1}{2}} \cdot d_{j+\frac{1}{2}} > 0$) cell, then we define d_j such that $|d_j - r^{'}(x_j)| = O(h^2)$ in smooth regions and $\max(\tilde{r}_j^{'}(x_{j-\frac{1}{2}}), \tilde{r}_j^{'}(x_{j+\frac{1}{2}})) = O(1)$. In transition cells we consider $d_0 = 0$.

Using PPH reconstructions and the discussions of the previous sections we can find the reconstructions r_j [3], [4].

To complete the schemes, Shu and Osher developed a special family of Runge-Kutta time integration schemes that have a TVD property [42], [43]. The TVD property prevents the time stepping scheme from introducing spurious spatial oscillations into upwind-biased spatial discretization.

For more details and numerical examples we refer [3], [4]. For instance, the PPH reconstruction presented in [3] is, for non-transition cells $d_{j-\frac{1}{2}} \cdot d_{j+\frac{1}{2}} > 0$, a polynomial of degree two corresponding to the grid data v_j, $d_j := \frac{2d_{j-\frac{1}{2}} \cdot d_{j+\frac{1}{2}}}{d_{j-\frac{1}{2}} + d_{j+\frac{1}{2}}}$ and $d_\theta := \operatorname{sgn}(d_{j-\frac{1}{2}}) \min\{|d_{j-\frac{1}{2}}|, |d_{j+\frac{1}{2}}|\}$. Indeed

$$p_j(x) = a_0 + a_1 x + a_2 x^2, \tag{24}$$

where:

$$a_2 = \frac{1}{2}\frac{d_\theta - d_j}{x(\theta) - x_j},$$

$$a_1 = d_\theta - x(\theta)\frac{d_\theta - d_j}{x(\theta) - x_j},$$

$$a_0 = v_j - \frac{h^2}{12}a_2,$$

$$\theta = \begin{cases} j - \frac{1}{2}, & |d_{j-\frac{1}{2}}| \leq |d_{j+\frac{1}{2}}|, \\ j + \frac{1}{2}, & |d_{j-\frac{1}{2}}| > |d_{j+\frac{1}{2}}|. \end{cases}$$

For transition cells ($d_{j-\frac{1}{2}} \cdot d_{j+\frac{1}{2}} \leq 0$), the only change is $d_1 := 0$.

In figures 1-4, for the Euler equations of gas dynamics [37], we study the initial condition:

$$u(x,0) = \begin{cases} (4.4, 2.3, 5) & -0.5 < x \leq -0.3 \\ (p(x), p(x), p(x)) & -0.3 < x < 0 \\ (0.5, 0, 2.5) & 0 \leq x < 0.5 \end{cases}$$

where $p(x) = \sin(40 \cdot \pi \cdot x)$.

We denote by $h = (b-a)/n$ the spatial discretization parameter and by m the number of time steps.

The fine structure in the density profile makes necessarily the use of high order methods. This problem is difficult for chock capturing methods because both high order accuracy and an oscillation free shock are needed. The CFL number, that is to say the relation between the parameters h and Δt, defines the stability of the numerical scheme. All explicit methods are sensitive to this number. Nevertheless, in order to compare the sensitive of the different methods, we consider different parameters sizes. ENO schemes [35] seems the most sensitive, since produce artificial oscillations. Nevertheless, both PHM [37] and PPHM converges to the entropy solution without fictitious oscillations (even in the worst case, see figure 4).

More results can be found in [3]. These numerical results seem to indicate that the PPH method has two main advantages with respect to the same order ENO schemes: it is not very sensitive neither to the CFL number nor to the discretization parameter and it is more local than ENO-3 in the sense that numerical flux depend on less variables (four and six respectively). Moreover, in the presence of discontinuities it is stable and with lower viscosity. The main advantage respect to the PHM scheme [37] is the

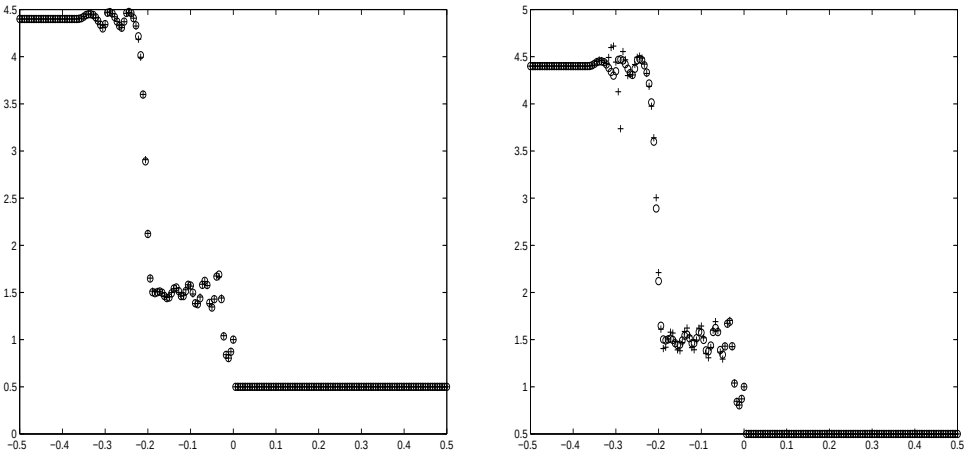

Figure 1: n=180, m=80, CFL=0.4, o=PPHM, left +=PHM, right +=ENO-3

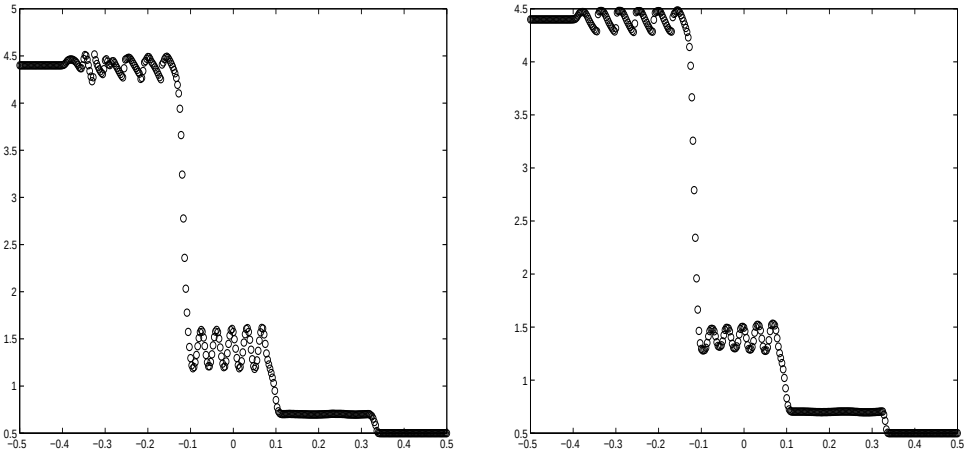

Figure 2: n=360, m=320, CFL=0.4, left ENO-3, right PHM

simplicity of our reconstruction, thus, it is less expensive. The CPU time used by the reconstruction in the PPH method is more or less 35% minor than the used in the others cases.

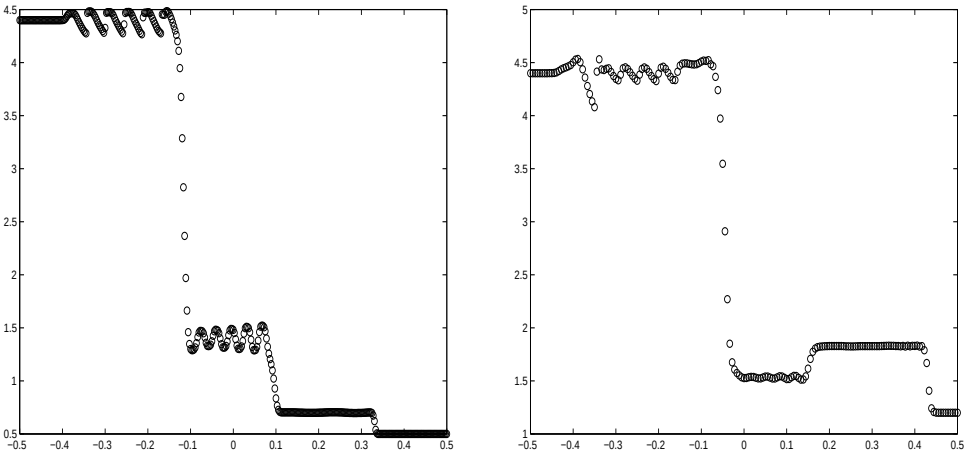

Figure 3: left n=360, m=320, CFL=0.4, PPHM right n=180, m=225, CFL=0.4, ENO-3

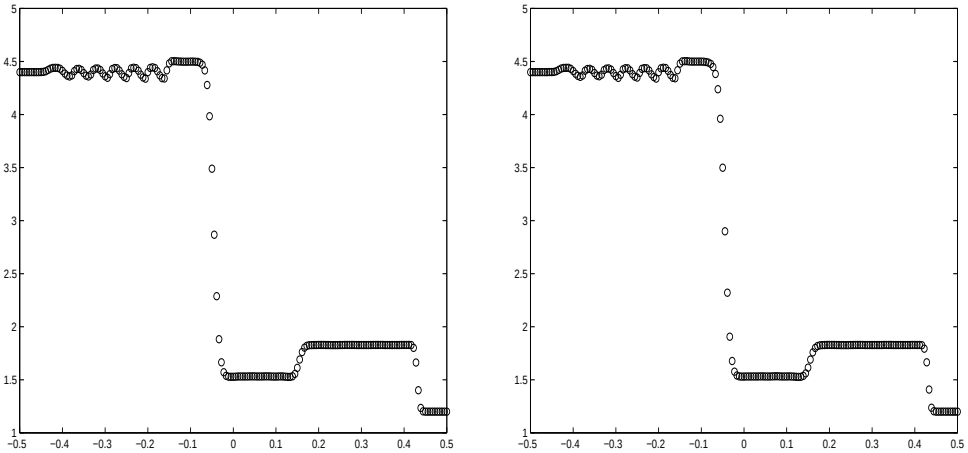

Figure 4: n=180, m=225, CFL=0.4, left PHM, right PPHM

4.2 Compression of locally oscillatory signals with discontinuities

Neither local techniques (based on multiscale decompositions) nor global ones (based on Fourier Analysis) have good compression properties for locally oscillatory signals with discontinuities. In this section we present a combined approach. We consider the PPH reconstruction (stable and adapted to the presence of discontinuities, as we have analyzed in the pre-

vious section) together with a discrete Fourier transform for the oscillatory parts of the considered signal. A similar idea has been used in [26], but using ENO (essential non oscillatory) interpolation as nonlinear interpolation technique. The problem of this type of nonlinear interpolation is the stability (ENO schemes are not stable [21]).

Following [26], we can define the so called *combined approach* as:

1) Determine and label the limits of each oscillatory interval I_m.

2) Compute the multiresolution of f^L.

3) Compress this representation. Let ϵ be the truncation parameter, used as

$$\tilde{d}_j^k = \mathbf{tr}(d_j^k, \epsilon) = \begin{cases} 0 & |d_j^k| \leq \epsilon \\ 0 & x_j^k \in I_m \\ d_j^k & otherwise \end{cases}$$

where d_j^k represents the different detail coefficients, assuming that the same value of ϵ for all the levels of multiresolution is used.

4) Compute the error between the reconstruction at the coarsest resolution level 0 and the original signal.

$$E_j = f_j^L - R_0(x_j^L).$$

5) Compute locally the DFT (Discrete Fourier Transform) of the finite sequence $\{E_j\}$ for the j such that $x_j^L \in I_m$.

6) Compress the coefficients A_j^m and B_j^m of the DFT representation,

$$\tilde{C}_j^m = \mathbf{tr}(C_j^m, \epsilon^F) = \begin{cases} 0 & |C_j^m| \leq \epsilon^F \\ C_j^m & otherwise \end{cases}$$

At the end we have the following representation of f^L:

$$\{f^0, (\tilde{d}^1, \tilde{d}^2, \ldots, \tilde{d}^L), \tilde{A}_j^m, \tilde{B}_j^m\}.$$

We consider a locally oscillatory signal with a discontinuity:

$$f(x) = \begin{cases} sin(0.2x) & x \in [-2\pi, 0) \cap [2\pi, 4\pi) \\ sin(0.2x) + 0.2sin(10x) & x \in [0, 2\pi) \\ sin(0.2x) + 1 & otherwise \end{cases} \tag{25}$$

We consider LIN4-The 4-point linear Delauries and Dubuc interpolatory wavelet transform, DFT-Discrete Fourier Transform, PPH-The 4 point nonlinear PPH multiresolution transform and the combined approach PPH-DFT.

In table 1 we observe the good properties of the combined approach. The highest compression is achieved by the PPH-DTF reconstruction. Figures 5-6 display the results, the jump discontinuity produces Gibbs-like phenomenon when using linear interpolation. The smallest error is produced by the PPH reconstruction but with 20 coefficients (corresponding to the oscillatory part) more than the combined approach.

$\epsilon = 0.001$, $L = 4$	LIN4	DFT	PPH	PPH-DFT
nnz	94	185	88	68
r_c	$3.67\ e-01$	$7.23\ e-01$	$3.44\ e-01$	$2.66\ e-01$
l_1	$14.39\ e+00$	$1.55\ e+00$	$2.82\ e-02$	$2.52\ e-01$
l_∞	$9.02\ e-01$	$4.40\ e-02$	$6.34\ e-04$	$1.55\ e-02$
l_2^2	$2.15\ e+00$	$1.56\ e-01$	$3.10\ e-03$	$4.09\ e-02$

Table 1: Number of non zero coefficients, compression ratio, l_∞, l_1 and l_2^2 prediction errors, function f_4, $(J_L + 1) = 257$ points, $\epsilon^F = 0.003$.

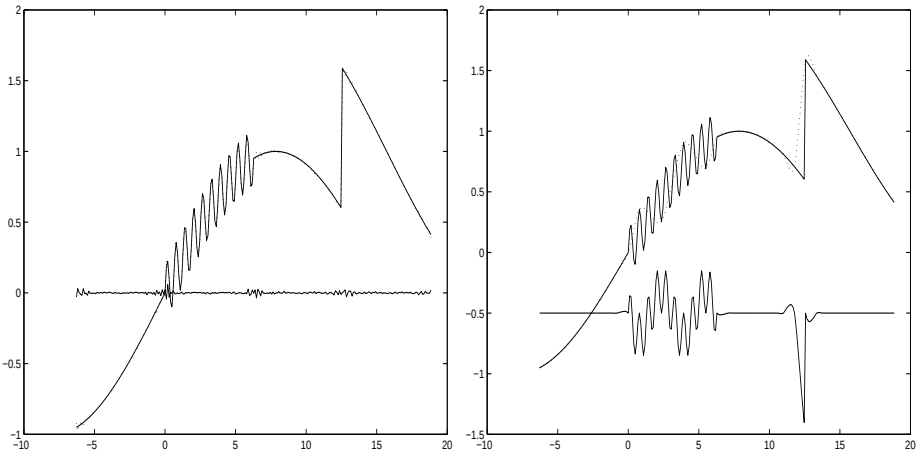

Figure 5: left DFT, right LIN4, original, reconstructed and error

For more details and numerical examples we refer [5].

4.3 Applications to image processing

In this section, we review the application of the PPH multiresolution scheme to compression and denoising of images.

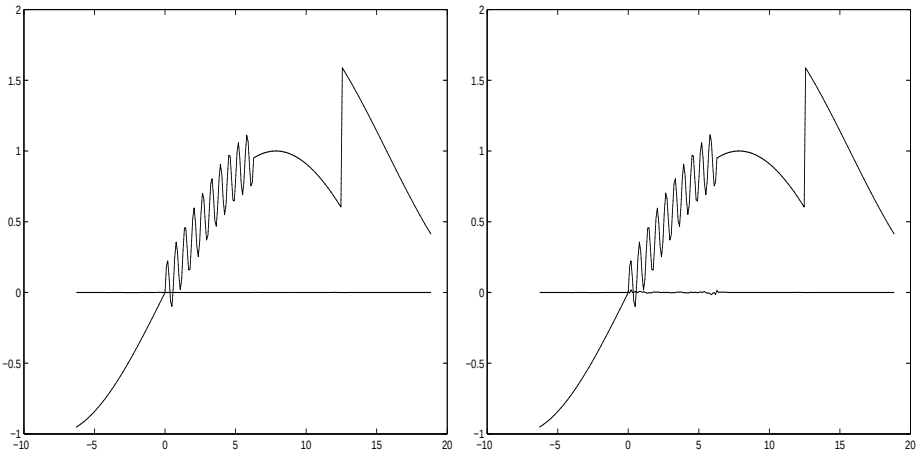

Figure 6: left PPH, right PPH-DFT, original, reconstructed and error

To analyze the compression properties of a two dimensional multiresolution algorithm M

$$A^k \leftrightarrow \left(\begin{array}{c|c} A^{k-1} & \Delta_2^k \\ \hline \Delta_3^k & \Delta_1^k \end{array} \right) \tag{26}$$

we introduce ϵ, a truncation parameter, and the truncation operator (*hard-threshold*) $\mathbf{tr}^\epsilon$ defined as

$$\mathbf{tr}^\epsilon(A^0, \Delta) = (A^0, \hat{\Delta}),$$

with

$$(\hat{\Delta}_l^k)_{ij} = \begin{cases} 0 & |(\Delta_l^k)_{ij}| \leq \epsilon, \\ (\Delta_l^k)_{ij} & otherwise. \end{cases}$$

The same value of ϵ is used for all multiresolution levels k. A different type of thresholding, more adapted to denoising applications, is the *soft-threshold* method [27]

$$\hat{\Delta}_i^k = \eta_\epsilon\left(\Delta_i^k\right) = sgn\left(\Delta_i^k\right) * \max\left(abs(\Delta_i^k) - \epsilon, 0\right).$$

After truncation, the inverse multiresolution transform M^{-1} is applied to obtain

$$\hat{A}^L = M^{-1}\mathbf{tr}^\epsilon(MA^L),$$

which is then compared to the original image using the following norms

$$\begin{aligned} ||A^L - \hat{A}^L||_{l_p} &= \left(\frac{1}{(J_L+1)^2} \sum_i |A_i^L - \hat{A}_i^L|^p \right)^{1/p}, \quad p = 1, 2, \\ ||A^L - \hat{A}^L||_{l_\infty} &= \max_i (|A_i^L - \hat{A}_i^L|). \end{aligned}$$

In order to obtain acceptable results the stability of the PPH multiresolution, analyzed in the previous sections, is crucial.

The compression ratio is defined as in [33], [34] by

$$r_c = \frac{nnz}{(J_L+1) \times (J_L+1) - (J_0+1) \times (J_0+1)},$$

where nnz denotes the number of non zero detail coefficients. Note that the smaller r_c, the larger the compression achieved.

On the other hand, the multiresolution thresholding procedure aims to remove noise by thresholding only the coefficients of the detail subbands while keeping the low resolution coefficients unaltered. As proved in [27], the soft-threshold can be considered the optimal procedure, from an statistical point of view, for denoising applications.

To perform the best denoisng results we have used the *soft-threshold* method varying the threshold value in each subband and in each scale in the following way:

$$\begin{aligned} \epsilon_1^k &= 2 * \frac{\sigma \sqrt{2 \ln(M_1^k)}}{(k+1) * (k+1)} \\ \epsilon_2^k &= \frac{\sigma \sqrt{2 \ln(M_2^k)}}{(k+1) * (k+1)} \\ \epsilon_3^k &= \frac{\sigma \sqrt{2 \ln(M_3^k)}}{(k+1) * (k+1)} \end{aligned}$$

where M_1^k, M_2^k, M_3^k are respectively the size of the matrix Δ_1^k , Δ_2^k and Δ_3^k, $k = 1, 2, \ldots, L$, and σ^2 denotes the noise variance of the image.

The choice of ϵ_1^k is justified by the fact that the Δ_1^k subband contains most of the detail information.

The threshold determines how much noise we want to suppress, and the larger the variance of the noise, the larger should it be.

4.3.1 Separable framework

Our test concerns the cameraman image, displayed in Figure 7.

Figure 7: Cameraman image

For this numerical test we consider $J_L = 256$ (the size of the image is 257×257) where $L = 4$ (finest level of resolution) and $\epsilon = 10$ (truncation parameter). We consider both linear (LIN4-The 4-point linear Delauries and Dubuc interpolatory wavelet transform) and nonlinear (PPH-Our 4 point nonlinear PPH multiresolution transform) tensor-product schemes. A zoom of the reconstructed images on an edge-dominated region is displayed in Figure 8. The PPH algorithm leads to a reconstructed image free of numerical artifacts or blurred regions. The numerical values in Table 2 are also consistent with our observations, and the PPH leads to better relation between r_c and quality of the reconstructed image.

$\epsilon = 10$	LIN4	PPH
nnz	12580	12100
r_c	$1.91e-01$	$1.84e-01$
l_1	3.82	3.25
l_∞	31.30	29.93
l_2	5.23	4.56

Table 2: Cameraman image ($J_L = 256$): Number of non zero coefficients, compression ratio, l_∞, l_1 and l_2 norms of compression error.

Figure 8: Upper-left Original, upper-right LIN4, bottom PPH, $L = 4$, $\epsilon = 10$

More images examples and discussion can be found in [9].

4.3.2 Nonseparable (Quincunx) framework

For an optimal representation of the edges, it is crucial to develop nonlinear schemes which are not based on tensor product. In [7], we link the non separable quincunx pyramid and the nonlinear discrete Harten's multiresolution framework. In order to obtain the stability of these representations, some new multiresolution processing algorithms was introduced.

First, we introduce a Harten's multiresolution analysis in $[0, 1] \times [0, 1]$ which admits a quincunx pyramid as a decomposition algorithm.

The transform $T(x,y) = (x+y, x-y)$ defines the sub-sampling grid of the quincunx pyramid. Note that $T^2 = 2Id$, which is the basic sub-sampling of the dyadic algorithm. Thus, in practice, the finest resolution level L is considered even.

Let $X^L = \{x_i^L, y_j^L\}_{i,j=0}^{J_L}$, $x_i^L = ih_L$, $y_j^L = jh_L$, $h_L = 2^{-L}h_0$, $J_L = 2^L J_0$, J_0 some integer, $h_0 = \frac{1}{J_0}$, L even.

Since $T^2 = 2Id$, we obtain, for $i,j = 0,\ldots,\frac{J_L}{2}$, $x_{2i}^L = x_i^{L-2}$ and $y_{2j}^L = y_j^{L-2}$.

The connections between L and $L-1$ or $L-1$ and $L-2$ are more elaborate. For the first step, we have for $j = 0,\ldots,J_L$

$$\begin{aligned}(x_{2i}^L, y_j^L) &= (x_i^{L-1}, y_j^{L-1}), \quad i = 0,\ldots\frac{J_L}{2}\ j\ even,\\ (x_{2i-1}^L, y_j^L) &= (x_i^{L-1}, y_j^{L-1}), \quad i = 1,\ldots\frac{J_L}{2}\ j\ odd,\end{aligned}$$

and for the second

$$(x_i^{L-1}, y_{2j}^{L-1}) = (x_i^{L-2}, y_j^{L-2}), \quad i,j = 0,\ldots\frac{J_L}{2}.$$

The following steps are performed similarly.

We consider

$$\mathcal{D}_k : \mathcal{C}([0,1]\times[0,1]) \longrightarrow V^k \qquad \bar{f}_{i,j}^k = (\mathcal{D}_k f)_{i,j} = f(x_i^k, y_j^k), \tag{27}$$

where if k is even $0 \le i,j \le J_k$, with $J_k := \frac{J_L}{2^{\frac{L-k}{2}}}$ and if k is odd $0 \le j \le 2J_k$ and

$$\begin{aligned}&0 \le i \le J_k,\ j\ even,\\ &1 \le i \le J_k,\ j\ odd,\end{aligned}$$

with $J_k := \frac{J_L}{2^{\frac{L-k+1}{2}}}$.

In this case, $\dim V^k = (J_k+1)\times(J_k+1)$ or $\dim V^k = ((J_k+1)\times(J_k+1)) + (J_k \times J_k)$ respectively. The decimation operators are for k even

$$\begin{aligned}\bar{f}_{i,j}^{k-1} &= (D_k^{k-1}\bar{f}^k)_{i,j} = \bar{f}_{2i,j}^k, \quad j\ even,\\ \bar{f}_{i,j}^{k-1} &= (D_k^{k-1}\bar{f}^k)_{i,j} = \bar{f}_{2i-1,j}^k, \quad j\ odd,\end{aligned}$$

and for k odd

$$\bar{f}_{i,j}^{k-1} = (D_k^{k-1}\bar{f}^k)_{i,j} = \bar{f}_{i,2j}^k.$$

In particular, we obtain for k even

$$\mathcal{N}(D_k^{k-1}) = \{v^k \in V^k \ : \ v^k_{2i,j} = 0, \ j \ even, \ v^k_{2i-1,j} = 0, \ j \ odd\},$$

and for k odd

$$\mathcal{N}(D_k^{k-1}) = \{v^k \in V^k : v^k_{i,2j} = 0\}.$$

Thus, if we denote by e^k the prediction errors, we will need to keep $e^k_{2i-1,j}$ j even, $e^k_{2i,j}$ j odd and $e^k_{i,2j-1}$ respectively.

A reconstruction procedure for this discretization is given by any operator $\mathcal{R}_k$ such that

$$\mathcal{R}_k : V^k \longrightarrow \mathcal{C}([0,1] \times [0,1]); \qquad \mathcal{D}_k \mathcal{R}_k \bar{f}^k = \bar{f}^k, \tag{28}$$

which means

$$(\mathcal{R}_k \bar{f}^k)(x^k_i, y^k_j) = \bar{f}^k_{i,j} = f(x^k_i, y^k_j). \tag{29}$$

Therefore, $\mathcal{R}_k$ should be a continuous function that interpolates the data $\bar{f}^k$ at the grid points of X^k. Finally, we define the prediction operators by

$$P^k_{k-1} := \mathcal{D}_k \mathcal{R}_{k-1}. \tag{30}$$

We have presented [7] a simple quincunx-PPH reconstruction, using the one dimensional PPH interpolation. For each detail, we choose between two principal directions the direction with smaller divided difference in absolute value (see figure 9), and then we apply the PPH reconstruction in 1-D. Due to this nonlinearity we use an error-control algorithm in order to ensure the stability.

Figure 9: *The circles are used to predict the square. For k even, right: reconstruction from level $k-2$ to $k-1$, left: reconstruction from level $k-1$ to k.*

The idea of a modified-encoding to deal with nonlinear multiresolution schemes is due to Harten. One dimensional algorithms in several settings can be found in [15], [33]. We modify the direct transform in such a way that the error accumulated in processing the values of the originally multi-scale

representation remains under a prescribed value. The goal of this procedure is to keep track of the accumulation error in processing the values in the multi-scale representation. The idea is to ensure a prescribed accuracy by intertwining the decomposition and the thresholding process. The details depend on the thresholding error at coarser levels. The full algorithm in the quincunx framework can be found in [7].

We perform a comparative study using the $PSNR$ (Peak Signal Noise Ratio) quality image indicator [41]. We recall that for an 8 bit image $(0 - 255)$,

$$PSNR = 20 \log_{10} \left(\frac{255}{||f^L - \hat{f}^L||_{l_2}} \right)$$

In table 3 the $PSNR$ versus the number of non zero coefficients is considered, and one can observe that for a given level of quality the compression attained by quincunx-PPH with error-control is higher than classical linear tensor product of the same order.

The goal of nonlinear-quincunx reconstruction operators is to improve the accuracy of the prediction in the vicinity of isolated singularities. A better treatment of the singularities corresponding to the image edges and therefore an improvement on the sparsity of the multiresolution representation of images are then expected.

PSNR	LIN4	PPH-Quincunx (E-C)
30	9481	3559
35	14147	7635
40	21518	12922
45	32430	19015

Table 3: Cameraman image, Number non-zero details, $L = 4$, Quincunx

More details can be found in [7].

4.3.3 Denoising of images

In this subsection, we present other possible application of the PPH multiresolution scheme: denoising, that is, the removal of noise from noisy data to obtain the unknown signal. As we said, we use the Donoho's soft-threshold which is the best candidate from a statistical point of view.

We define r_{scheme} as the $PSNR$ number between the denoised picture and the original one, and we compute $R_{PPH/LIN4} = \frac{r_{PPH}}{r_{LIN4}}$.

We consider different noise levels varying between 10 and 50.

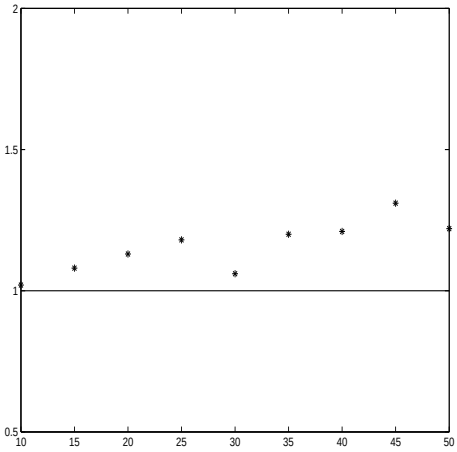

Figure 10: cameraman image, $R_{PPH/LIN4}$ vs. noise level

The PPH obtains the best results (better $PSNR$ for all the noise levels considered). The proper adaptation of this technique to the presence of edges improves the image denoising procedure.

See [8] for more experiments and details.

5 Conclusions and current research

In this paper, a fully nonlinear reconstruction operator in Harten's multiresolution framework has been reviewed. The corresponding nonlinear multiresolution algorithm has been analyzed in terms of accuracy and stability. Numerical approximation of hyperbolic conservation laws using the PPH upwind scheme based on fluxes and the Shu-Osher third order TVD Runge-Kutta method seems to work very well. In presence of discontinuities it is stable and with low viscosity. A combined approach based on local techniques, with a specific adaptive treatment of discontinuities for the slowly varying part of the signal, and global techniques (applied locally), derived from Fourier decompositions, to represent the oscillatory part has been analyzed. Finally, several image processing applications are presented. Edge resolution, robustness with regard to texture or noise, accuracy and compression rate have been investigated. One should mention that in our calculations the CPU time related to the PPH scheme remains, up to 4%, equivalent to the CPU time associated to the linear scheme.

Our group is collaborating in some other PPH research issues:

- Extension of PPH's ideas to the cell-average setting.
- Definition and analysis of new nonlinear reconstruction operators of high order.
- Generalization of the stability analysis in order to include general families of schemes.
- Definition and analysis of PPH schemes of Hermite's type.
- Application of nonlinear schemes for color images processing.
- ...

Acknowledgments

We would like to thank all coauthors, who worked with me on the PPH reconstructions, for useful discussions and suggestions. They are: I.Ali, S.Busquier, V.F.Candela, H.Cherif, K.Dadourian, R.Donat, D.El Kebir, J.Liandrat, J.Molina and J.C.Trillo. Finally, we also want to thank the referees and the editor for their suggestions.

References

[1] Ali I., Amat S. and Trillo J.C., (2006). Point values Hermite multiresolution for non-smooth noisy signals. *Computing*, **77** 3, 223–236.

[2] Amat S., Aràndiga F., Cohen A. and Donat R., (2002). Tensor product multiresolution analysis with error control for compact image representation. *Signal Processing*, **82**(4), 587-608.

[3] Amat S., Busquier S. and Candela V.F., (2003). A polynomial approach to Piecewise Hyperbolic Method, *Int.J. Computational Fluid Dynamics* **17**(3), 205-217.

[4] Amat S., Busquier S. and Candela V.F.,, (2003). Local Total Variation Bounded methods for hyperbolic conservation laws, *J. of Comp. Methods in Sciences and Engineering*, **3**(3), 193-200.

[5] Amat S., Busquier S., El Kebir D. and Molina J., (2002). Compression of locally oscillatory signals with discontinuities, *International Mathematical J.*, **2**(12), 1141-1156.

[6] Amat S., Busquier S. and Trillo J.C., (2005). Stable Interpolatory Multiresolution in 3D , *Applied Numerical Analysis and Computational Mathematics*, **2**(2), 177-188.

[7] Amat S., Busquier S. and Trillo J.C., (2005). Non-linear Harten's Multiresolution on the Quincunx Pyramid , *J. of Comp. and App. Math.*, **189** (1-2), 555-567.

[8] Amat S., Cherif H. and Trillo J.C., (2005). Denoising using Linear and Nonlinear Multiresolutions, *Engineering of Computations*, **22** 7, 877-891.

[9] Amat S., Donat R., Liandrat J. and Trillo J.C., (2006). Analysis of a new nonlinear subdivision scheme. Applications in image processing. *Foundations of Computational Mathematics*, **6** 2, 193–225.

[10] Amat S., Donat R., Liandrat J. and Trillo J.C., (2005). A fully adaptive PPH multiresolution scheme for image processing. *Mathematical and Computer Modelling*, to appear..

[11] Amat S. and Liandrat J., (2005). On the stability of the PPH nonlinear multiresolution, *Appl. Comp. Harm. Anal.*, **18**(2), 198-206.

[12] Aràndiga, F., Baeza, A. and Donat, R., (2004). Discrete multiresolution based on Hermite interpolation: computing derivatives. Recent advances in computational and mathematical methods for science and engineering. *Commun. Nonlinear Sci. Numer. Simul.*, **9** 2, 263–273.

[13] Aràndiga, F. and Belda, Ana M., (2004). Weighted ENO interpolation and applications. Recent advances in computational and mathematical methods for science and engineering. *Commun. Nonlinear Sci. Numer. Simul.*, **9** 2, 187–195.

[14] Aràndiga, F., Cohen, A., Donat, R. and Dyn, N., (2005). Interpolation and approximation of piecewise smooth functions. (English summary) *SIAM J. Numer. Anal.*, **43** 1, 41–57 (electronic).

[15] Aràndiga F. and Donat R., (2000). Nonlinear Multi-scale Decomposition: The Approach of A.Harten, *Numerical Algorithms*, **23**, 175-216.

[16] Binev, P., Dahmen, W., DeVore, R. and Dyn, N., (2004). Adaptive approximation of curves. Approximation theory: a volume dedicated to Borislav Bojanov, 43–57, Prof. M. Drinov Acad. Publ. House, Sofia.

[17] Cohen, A. Theoretical, applied and computational aspects of nonlinear approximation. (English summary) Multiscale problems and methods in numerical simulations, 1–29, Lecture Notes in Math., 1825, Springer, Berlin, 2003.

[18] Cohen, A. Numerical analysis of wavelet methods. Studies in Mathematics and its Applications, 32. North-Holland Publishing Co., Amsterdam, 2003.

[19] Cohen, A., Dahmen, W., Daubechies, I. and DeVore, R., (2001). Tree approximation and optimal encoding. *Appl. Comput. Harmon. Anal.*, **11** 2, 192–226.

[20] Cohen, A. and Dyn, N., (1996). Nonstationary subdivision schemes and multiresolution analysis. *SIAM J. Math. Anal.*, **27** 6, 1745–1769.

[21] Cohen A., Dyn N. and Matei B., (2003). Quasi linear subdivision schemes with applications to ENO interpolation. *Applied and Computational Harmonic Analysis*, **15**, 89-116.

[22] Dahmen, W. Multiscale and wavelet methods for operator equations. Multiscale problems and methods in numerical simulations, 31–96, Lecture Notes in Math., 1825, Springer, Berlin, 2003.

[23] Daubechies I., Runborg O. and Sweldens W., (2004). Normal multiresolution approximation of curves, *Const. Approx.*, **20** 3, 399–463.

[24] Deslauriers G. and Dubuc S., (1989). Symmetric iterative interpolation processes, *Const. Approx.*, **5**, 49-68.

[25] Donat, R. and Marquina, A., (1996). Capturing shock reflections: an improved flux formula. *J. Comput. Phys.*, **5** 1, 42–58.

[26] Donat R. and Harten A., (1993). Data compression Algorithms for Locally Oscillatory Data, UCLA CAM Report 93-26.

[27] Donoho D., (1995). Denoising by soft thresholding, *IEEE Trans. on Inform. Theory*, **41**(3), 613-627.

[28] Donoho D., Yu T.P.-Y, (2000). Nonlinear pyramid transforms based on median interpolation. *SIAM J. Math. Anal.*, **31**(5), 1030-1061.

[29] Dyn, N., Kuijt, F., Levin, D. and van Damme, R., (1999). Convexity preservation of the four-point interpolatory subdivision scheme. *Comput. Aided Geom. Design*, **16** 8, 789–792.

[30] Dyn, N. and Levin, D., (2002) Subdivision schemes in geometric modelling. *Acta Numer.*, **11**, 73–144.

[31] Dyn, N., Levin, D. and Luzzatto, A., (2003) Refining oscillatory signals by non-stationary subdivision schemes. Modern developments in multivariate approximation, 125–142, Internat. Ser. Numer. Math., 145, Birkhuser, Basel.

[32] Floater M. S. and Michelli C.A., (1998). Nonlinear stationary subdivision, *Approximation theory: in memory of A.K. Varna, edt: Govil N.K, Mohapatra N., Nashed Z., Sharma A., Szabados J.*, 209-224.

[33] Harten A., (1993). Discrete multiresolution analysis and generalized wavelets, *J. Appl. Numer. Math.* **12**,153-192.

[34] Harten A., (1996). Multi resolution representation of data II, *SIAM J. Numer. Anal.*, **33**(3), 1205-1256.

[35] Harten A., Osher S.J., Engquist B. and Chakravarthy S. (1987). Some results on uniformly high-order accurate essentially non-oscillatory schemes. *Appl. Numer. Math.*, **2**, 347-377.

[36] Kuijt F. and van Damme R., (1998). Convexity preserving interpolatory subdivision schemes. *Const. Approx.*, **14**, 609-630.

[37] Marquina, A., (1994). Local piecewise hyperbolic reconstruction of numerical fluxes for nonlinear scalar conservation laws. *SIAM J. Sci. Comput.*, **15** 4, 892–915.

[38] Matei, B., (2005). Smoothness characterization and stability in nonlinear multiscale framework: theoretical results. *Asymptot. Anal.*, **41** 3-4, 277–309.

[39] Matei, B., (2004). Denoising using nonlinear multiscale representations. *C. R. Math. Acad. Sci. Paris*, **338** 8, 647–652.

[40] Oswald P., (2004). Smoothness of Nonlinear Median-Interpolation Subdivision, *Adv. Comput. Math.*, **20**(4), 401-423.

[41] Rabbani M. and Jones P.W., (1991). Digital Image Compression Techniques. Tutorial Text, Society of Photo-Optical Instrumentation Engineers (SPIE), TT07.

[42] Shu C.W. and Osher S.J. (1987). Efficient implementation of essential non-Oscillatory shock capturing schemes, *J.Comput.Phys.*, 77, 231-303.

[43] Shu C.W. and Osher S.J. (1989). Efficient implementation of essential non-Oscillatory shock capturing schemes II, *J.Comput.Phys.*, 83, 32-78.

[44] Trillo, J.C. Multirresolución no lineal y Aplicaciones, PhD in the University of Valencia, Spain, 2006.